J. Fluid Mech. (1980), *vol.* 99, *part* 4, *pp.* 841–858
Printed in Great Britain

Self-similar explosion waves of variable energy at the front

By G. I. BARENBLATT,
Moscow Physico-Technical Institute and Institute of Oceanology,
U.S.S.R. Academy of Sciences, Moscow

R. H. GUIRGUIS,
University of California, Berkeley, U.S.A.

M. M. KAMEL,
Cairo University, Egypt

A. L. KUHL
R & D Associates, Marina del Rey, California, U.S.A.

A. K. OPPENHEIM,
University of California, Berkeley, U.S.A.

AND YA. B. ZEL'DOVICH
Institute of Applied Mathematics, U.S.S.R. Academy of Sciences, Moscow

(Received 5 July 1977 and in revised form 3 December 1979)

A set of self-similar solutions for blast waves associated with the deposition of variable energy at the front is presented. As a consequence of self-similarity, the results are applicable when the ambient atmosphere into which the wave front propagates is at a negligibly low pressure and temperature. Besides the class of (1) blast waves associated with energy gain that covers a regime bounded on one side by the well-known solution for adiabatic strong explosion waves (ASE) and, on the other side, by the solution for waves having the Chapman–Jouguet condition established immediately behind the front, included within the scope of our analysis are two others: (2) blast waves associated with energy loss that occupy a regime between the ASE solution and the case of infinite density ratio across the front, and (3) a non-unique class of solutions for blast waves associated with energy deposition that may have either locally sonic or supersonic flow immediately behind the front, extending over the regime between the waves headed by the Chapman–Jouguet detonation and the case of infinite rate of energy deposition. Specific results for a number of representative cases are expressed in terms of integral curves on the phase plane of reduced blast wave co-ordinates, as well as in the form of particle velocity, temperature, density, and pressure profiles across the flow field.

1. Background

The theory of strong explosion waves is founded upon the studies of Sedov (1945, 1946), Taylor (1950*a*, *b*) and von Neumann (1963). To begin with, they were concerned primarily with blast waves of constant energy, i.e. cases where, except for the

0022-1120/80/4487-1670 $02.00

initiation, no energy is deposited or withdrawn from the blast wave in the course of its propagation. The fronts of such waves are inert shocks.

This was enhanced by interest in blast waves headed by detonations, as exhibited by the writings of Zel'dovich (1942; see also Zel'dovich & Kompaneets 1955), Taylor (1950*b*) and Sedov (1957). Here additional energy is deposited in the blast wave as a consequence of the growth of the front surface across which a finite amount of energy per unit mass is released by an exothermic process. At first this energy was considered to be constant, resulting in a uniform front propagation speed. Later it was realized that the amount of energy deposited at the front may, in such cases, vary, say due to radiation losses, leading to the concept of blast waves headed by Chapman–Jouguet detonations of variable velocity of propagation. The condition of self-similarity imposes then a strict rule on the variation of the front-propagation speed, as first noted by Sapunkov (1967) and by Barenblatt & Sivashinsky (1970), brought up by Barenblatt & Zel'dovich (1971, 1972) and independently investigated by Oppenheim, Kuhl & Kamel (1972). Salient features of the fundamental background for these studies have been described in the text of Zel'dovich & Raizer (1966).

At the same time concern over blast waves associated with variable energy deposition at the front was spearheaded by interest in explosions produced by laser irradiation. The postulate that energy is deposited in such waves at a constant rate was considered to be physically realistic, and self-similar solutions derived independently by Champetier, Couairon & Vendenboomgaerde (1968), Freeman (1968), Wilson and Turcotte (1970) and Dabora (1972) proved to be, for all practical purposes, sufficiently accurate. A general treatment of such waves has been given by Raizer (1974), while some representative cases have been included in the parametric study of self-similar blast waves carried out by Oppenheim, Kuhl, Lundstrom & Kamel (1972).

With this as a background, it became of interest to carry out a comprehensive parametric study of self-similar solutions for blast waves for which variable energy is deposited at the front. The results of this study are reported here.

With respect to the physical significance of the subject of our studies, the following is worth noting. The family of solutions we expose bears a fundamental difference from the classical case of an adiabatic point explosion – the self-similar blast wave resulting from an instantaneous deposition of energy at a point. (The latter, incidentally, belongs to the family, occupying in fact a central position as the line of demarcation between blast waves driven by the deposition of energy and those associated with its withdrawal.) Whereas the self-similar solution for an adiabatic blast wave pertains to the initial stages of the flow field that later becomes non-self-similar, just the opposite holds true for all the other particular solutions of the family. The physical reason for this is that blast waves driven at the front have to be started by the deposition of energy over a finite element of space rather than at a point. As a consequence of the space dimension associated with this feature, such waves are essentially non-self-similar. However, as demonstrated by the results of numerical analysis (*viz.* Barenblatt 1978), as the time progresses the solutions become self-similar. Thus, in contrast to the classical case of an adiabatic point explosion, where the self-similar solution applies at early times, the self-similar solutions for blast waves driven at the front represent the asymptotic limit of initially non-self-similar flow fields attainable at late times.

2. Analysis

Physical space

Let r and t be, respectively, the physical space and time co-ordinates, p be the local pressure, ρ the density, and u the particle velocity. Consider the medium to behave essentially as a perfect gas with a constant specific-heat ratio, γ. Then, at any instant of time, the energy deposited in the blast wave per unit area in the plane-symmetrical case ($j = 0$), per unit polar angle and axial length in the line-symmetrical case ($j = 1$), and per unit steric angle in the point-symmetrical case ($j = 2$), is

$$E = \int_0^{r_n} \left(\frac{1}{\gamma - 1} \frac{p}{\rho} + \frac{u^2}{2} \right) \rho r^j \, dr, \tag{1}$$

where the subscript n denotes the front.

Postulate, as required for the sake of self-similarity, the existence of the invariant front-velocity index

$$\mu \equiv \frac{d \ln r_n}{d \ln t} = \frac{t}{r_n} w, \tag{2}$$

where w is the front velocity, and introduce the wave-power index

$$\epsilon \equiv \frac{d \ln E}{d \ln t} = \frac{t}{E} \mathscr{P}, \tag{3}$$

where $\mathscr{P}$ is the power of the wave, that is the rate at which energy is deposited in the wave.

Since the dimension of E, as defined above, is $[ML^jT^{-2}]$, one is led by dimensional considerations to the relationship

$$r_n = \left(\frac{\delta_j E}{J \rho_a t^\epsilon} \right)^{1/(j+3)} t^\mu, \tag{4}$$

where $\delta_j = 2\pi j + (j-1)(j-2)$, J is a non-dimensional factor whose value depends on the energy distribution within the wave, while subscript a refers to conditions of the ambient atmosphere.

By matching the dimensions of time in (4), one gets the following linear dependence between the two invariants

$$\epsilon = (j+3)\mu - 2, \tag{5}$$

while, with the aid of (2), (4) yields

$$J = \frac{\delta_j \mu^2 E}{\rho_a r_n^{j+1} w^2}. \tag{6}$$

It is one of the ultimate objectives of the analysis to evaluate the relationship between J and ϵ over the whole scope of self-similar solutions for point explosions of variable energy.

Phase space

As it is well known (see, for example, Guderley 1942; Courant & Friedrichs 1948; Sedov 1957; Zel'dovich & Raizer 1966), the solution of a self-similar problem can be reduced to the task of determining an integral curve on an appropriate phase plane. Particularly convenient as co-ordinates of such a plane are the following reduced variables:

$$F \equiv \frac{tu}{r\mu} = \frac{u}{xw}, \tag{7}$$

where $x \equiv r/r_n$, and

$$Z \equiv \left(\frac{ta}{r\mu}\right)^2 = \frac{rp}{x^2\rho w^2}, \tag{8}$$

where a is the local velocity of sound.

The governing equation can be expressed then simply as follows (Oppenheim, Kuhl, Lundstrom & Kamel 1972):

$$\frac{dZ}{dF} = \frac{Z}{1-F}\frac{\mathbb{P}(F, Z)}{\mathbb{Q}(F, Z)}, \tag{9}$$

where, for blast waves devoid of internal energy sources,

$$\mathbb{Q}(F, Z) \equiv (F_F - F)(1-F)F + (j+1)(F_D - F)Z, \tag{10}$$

$$\mathbb{P}(F, Z) \equiv (\gamma-1)\mathbb{Q}(F, Z) + [(j+1)(\gamma-1)+2](F_B - F)\mathbb{D}(F, Z), \tag{11}$$

while

$$\mathbb{D}(F, Z) \equiv (1-F)^2 - Z \tag{12}$$

and

$$F_F \equiv \mu^{-1}, \tag{13}$$

$$F_D \equiv \frac{2(\mu^{-1}-1)}{(j+1)\gamma}, \tag{14}$$

$$F_B \equiv \frac{2\mu^{-1}}{(j+1)(\gamma-1)+2}. \tag{15}$$

Once the integral curve for a given problem is determined, the location in the flow field of a given state, specified in terms of F and Z, can be evaluated by the quadrature of either of the two following relations

$$\frac{d\ln x}{dF} = \frac{\mathbb{D}(F, Z)}{\mathbb{Q}(F, Z)}, \tag{16}$$

or

$$\frac{d\ln x}{dZ} = \frac{1-F}{Z}\frac{\mathbb{D}(F, Z)}{\mathbb{P}(F, Z)}. \tag{17}$$

The velocity and temperature profiles are determined then directly from the definitions of F and Z, (7) and (8), namely

$$\frac{u}{u_n} = \frac{F}{F_n}x \tag{18}$$

and

$$\frac{T}{T_n} = \left(\frac{a}{a_n}\right)^2 = \frac{Z}{Z_n}x^2, \tag{19}$$

where subscript n denotes the state immediately behind the front. Finally, the density and pressure profiles can be obtained from the so-called adiabatic integral (Sedov 1957, Oppenheim, Kuhl, Lundstrom & Kamel 1972), yielding

$$\frac{R}{R_n} = \frac{\rho}{\rho_n} = \left[\frac{Z}{Z_n}\left(\frac{1-F}{1-F_n}\right)^{2(\mu^{-1}-1)/(j+1)}x^{2(\mu^{-1}-1)}\right]^{-(j+1)/[(j+1)(\gamma-1)+2(\mu^{-1}-1)]} \tag{20}$$

while

$$\frac{P}{P_n} = \frac{p}{p_n} = \frac{T}{T_n}\frac{R}{R_n}, \tag{21}$$

where

$$R \equiv \frac{\rho}{\rho_a} \tag{22}$$

so that $R_n = \rho_n/\rho_a$, and

$$P \equiv \frac{p}{p_n} \tag{23}$$

so that $P_n = p_n/p_a$.

Front

In order to satisfy the condition of self-similarity, the state immediately behind the front must be represented by a point on the locus of infinite pressure ratios (or temperature ratios) across the front, the $P_n = \infty$ line. In terms of the phase plane co-ordinates its equation is (Oppenheim, Kuhl, Lundstrom & Kamel 1972)

$$Z_n = \gamma(1 - F_n) F_n. \tag{24}$$

A point on the integral curve is related directly to the density ratio across the front since, from the definition of F, (7), and the continuity equation for the front, it follows that

$$F_n = 1 - R_n^{-1}. \tag{25}$$

At the same time the magnitude of the reduced variable specifies the amount of energy deposited at the front per unit mass, q, since from the energy equation for the front, combined with (24),

$$\omega \equiv \frac{q}{W^2} = \frac{1}{2\beta}(F_A - F_n) F_n, \tag{26}$$

where

$$\beta \equiv (\gamma_n - 1)/(\gamma_n + 1). \tag{27}$$

while

$$F_A = 1 - \beta. \tag{28}$$

The relationship prescribed by (26) is displayed in figure 1 for different values of γ_n. From the above it is readily evident that for $F_n < F_A$ the change of state across the front is associated with energy deposition, while for $F_n > F_A$, with energy withdrawal. The co-ordinate F_A corresponds to the adiabatic strong explosion solution, for which $\omega = 0$, while the maximum value of ω is obtained for the Chapman–Jouguet condition for which $F_n = F_j = \frac{1}{2}(1 - \beta) = (\gamma_n + 1)^{-1}$. Locus of points satisfying this condition is delineated in figure 1 by a chain-dotted line.

The magnitude of F_n specifies also the temperature immediately behind the front, since from the definition of Z, (8), and the equation for the $P_n = \infty$ line, (24), one has

$$\tau \equiv \frac{\mathscr{R}T}{w^2} = \frac{1}{\gamma} Z_n = (1 - F_n) F_n, \tag{29}$$

where $\mathscr{R}$ is the gas constant per unit mass. The above relation is represented by a broken line in figure 1. It is of interest to note that, as a rule, τ reaches maximum at a higher value of F_n than that corresponding to the Chapman–Jouguet condition.

Now, the energy contained in the flow field of the wave as a consequence of that deposited per unit mass at its front

$$E = \int_0^{r_n} q\rho_a r^j dr = \omega\rho_a \int_0^{r_n} w^2 r^j dr \tag{30}$$

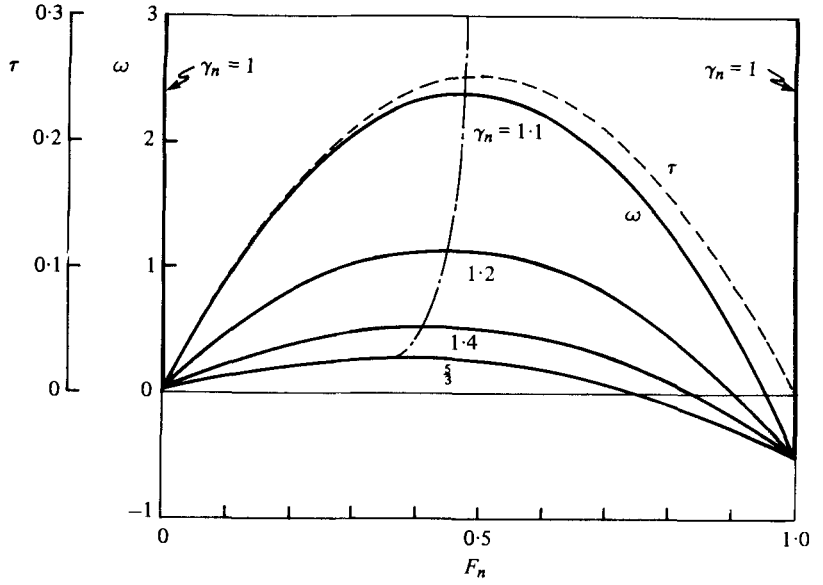

FIGURE 1. Non-dimensional parameters for energy deposited at the front $\omega \equiv q/w^2$, and temperature immediately behind it, $\tau \equiv \mathscr{R}T/w^2$, as unique functions of its reduced co-ordinate, F_n.

can be expressed in non-dimensional form, according to (6), as follows:

$$J = \frac{\delta_j \mu^2 \omega}{r_n^{j+1} w^2} \int_0^{r_n} w^2 r^j dr$$

$$= \delta_j \mu^2 \omega \int_0^1 x^{j+2-2\mu^{-1}} dx$$

$$= \frac{\delta_j \mu^2 \omega}{j+3-2\mu^{-1}}. \tag{31}$$

It should be noted that in the derivation shown above advantage has been taken of the fact that, as a consequence of the definition of μ, (2), $w \propto \mu r^{1-\mu^{-1}}$. Finally, by virtue of (5), taking into account the definition of (26), one gets

$$J = \frac{\delta_j \mu^3 \omega}{\epsilon} = \frac{\delta_j}{2\beta\epsilon}\left(\frac{\epsilon+2}{j+3}\right)^3 (F_A - F_n) F_n. \tag{32}$$

Solution

Each integral curve is associated with a saddle-point singularity, D, corresponding to conditions at the centre of the wave. Its position on the phase plane is specified by F_D given by (14), while $Z_D = \infty$. The slope of the integral curve at D is evaluated by expressing (9) in terms of Z^{-1} and applying the l'Hospital rule. This yields

$$\left(\frac{dZ^{-1}}{dF}\right)_D = \frac{[(j+1)\gamma\mu]^3[(j+1)(j+3)\gamma\mu - 4(1-\mu)]}{2[(j+1)\gamma\mu - 2(1-\mu)]^2[(j+1)\gamma - 2(1-\mu)](1-\mu)}. \tag{33}$$

With proper care taken of singularity D and of the limits of extrema expressed by the conditions $\mathbb{P}(F, Z) = 0$ and $\mathbb{Q}(F, Z) = 0$, the integration of the governing equation (9) can be carried out by a conventional (say Runge–Kutta) numerical technique.

For the starting step in the vicinity of singularity D, (33) is used. At the same time, the relationship between the points of an integral curve and the space co-ordinate x is established by quadrature of either (16) or (17) depending whether dF/dZ is larger or smaller than unity. As a consequence of the form of these equations, one has to assign at first in the vicinity of D an arbitrary initial value for x. This is then adjusted so that $x = 1$ at the intersection of the integral curve with the $P_n = \infty$ line. As the integral curves are evaluated, space profiles of the gasdynamic parameters are determined by the use of (18), (19), (20) and (21).

Finally the non-dimensional energy integral, appearing as the energy distribution factor in (4), is calculated according to the following expression obtained from (1), (6), (7), and (8)

$$J = \delta_j \mu^2 \int_0^1 \left[\frac{Z}{\gamma(\gamma-1)} + \frac{F^2}{2}\right] R(F, Z)\, x^{j+2}\, dx. \tag{34}$$

The integration is performed, of course, along a fixed integral curve. Since each integral curve is associated with a particular value of μ and hence, by virtue of (5), a specific value of ϵ, this yields a direct relationship between J and ϵ.

The accuracy of the results are checked in two ways. First by the condition imposed by the global mass conservation principle, namely

$$\int_0^1 R(F, Z)\, x^j\, dx = (j+1)^{-1}. \tag{35}$$

Secondly, this can be done by invoking the energy conservation principle, according to which the result of (34) has to be in agreement with that of (32), the values of F_n appearing in the latter having been obtained from the intersection of the integral curve with the $P_n = \infty$ line. The results of this check are described in the next section.

3. Results

Integral curves for the spherical case of $j = 2$ and a perfect gas with $\gamma = 1{\cdot}4$, corresponding to a representative set of values of the power index, ϵ, or the velocity index, μ, are depicted in figure 2. Shown there also is the sonic line $\mathbb{D}(F, Z) = 0$ according to (12), and the locus of states immediately behind the front, the $P_n = \infty$ line given by (24). Moreover, represented by broken lines are loci of constant x obtained by interpolation of the values of this parameter as it was determined in the course of numerical integration.

The pivotal line in the set is that for $\epsilon = 0$, the well-known solution for an adiabatic strong explosion. On the left of it are solutions for point explosions associated with energy deposition at various rates, up to the limiting case of infinite power. On the right are solutions for blast waves associated with energy withdrawal. They are terminated by the line $F = 1$, corresponding to the extreme case of infinite density ratio across the front. This imposes a lower bound upon the velocity index, μ, and, by virtue of (5), the power index, ϵ, that follows directly from the condition $F_n = F_D = 1$, which, according to (14), yields $\mu = 2/[(j+1)\gamma + 2]$. The numerical values of this bound for the case of $\gamma = 1{\cdot}4$ are indicated on top of figure 2.

As they appear in figure 2, starting from the integral curve for $\epsilon = \epsilon_J = 1{\cdot}6$ (or $\mu = \mu_J = 0{\cdot}72$), all the rest (i.e. those for $\epsilon > \epsilon_J$) pass through the point of intersection

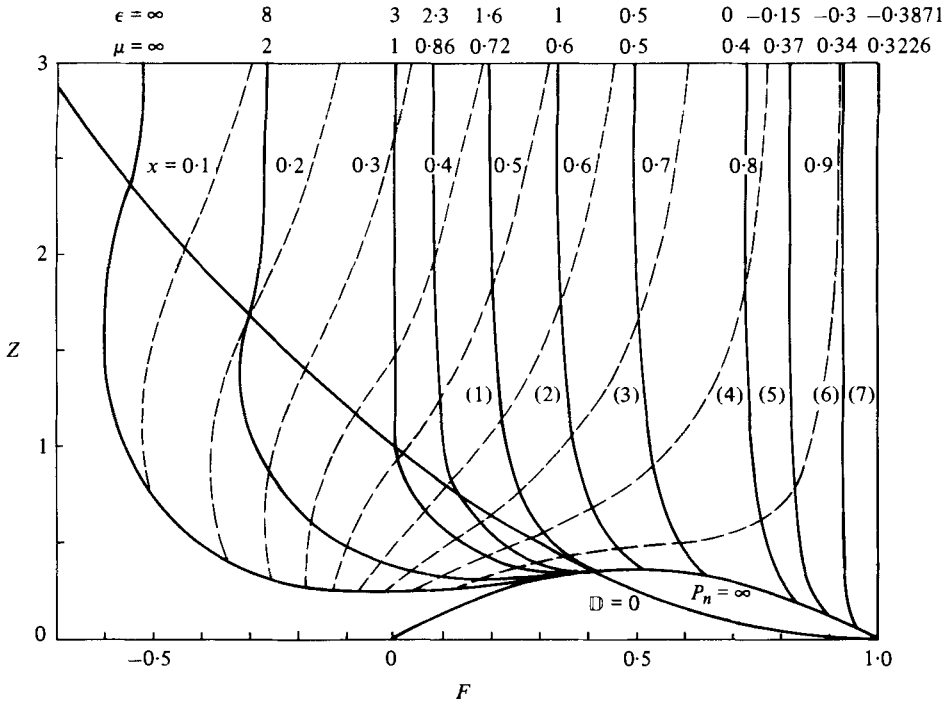

FIGURE 2. Representative integral curves on the phase plane ($j = 2$, $\gamma = 1{\cdot}4$).

between the locus of $P_n = \infty$ and the $\mathbb{D} = 0$ line, representing the Chapman–Jouguet condition. However, these solutions are not unique;† for the same value of the velocity index, μ, as well as the power index, ϵ, one has a whole family of solutions, the members of which correspond to any value of F_n within the range $0 \leqslant F_n < (F_n)_J$, where, for our case of $j = 2$ and $\gamma = 1{\cdot}4$, $(F_n)_J = 0{\cdot}416667$. By virtue of (26), this, in turn, corresponds to any value of ω within the range $0 \leqslant \omega \leqslant \omega_J$, where, for $j = 2$ and $\gamma = 1{\cdot}4$, $\omega_J = 0{\cdot}520833$. Displayed in figure 3 are six solutions within each of four families for which, respectively, $\epsilon = 2{\cdot}3$, 3, 8 and ∞ (or $\mu = 0{\cdot}86$, 1, 2, and ∞). The six are in all cases made up of those corresponding to

$$F_n = 0{\cdot}416667, \quad 0{\cdot}3, \quad 0{\cdot}2, \quad 0{\cdot}1, \quad 0{\cdot}01, \quad 0,$$

or

$$\omega = 0{\cdot}520833, \quad 0{\cdot}48, \quad 0{\cdot}38, \quad 0{\cdot}22, \quad 0{\cdot}0247, \quad 0.$$

It should be observed that the terminal case of $F_n = \omega = 0$ corresponds to infinite front velocity, since, in view of the finite rate of energy deposition in the various families for $\epsilon_J < \epsilon < \infty$, the rate of energy deposition is finite and consequently $q \neq 0$.

For all these cases the flow immediately behind the front is locally supersonic with respect to it. At any point in the flow field the flow is considered to be locally supersonic or subsonic depending on whether the relative particle velocity with respect to that of the locus of constant x, i.e. $(\partial r/\partial t)_x$, is larger or smaller than the local velocity of sound. In general, for all the points on the $\mathbb{D} = 0$ line the flow is in this sense locally sonic, below it is supersonic while above subsonic. Thus, for all the solutions displayed in figure 3, the flow behind the front is locally supersonic until, at the state represented

† A property pointed out by Barenblatt & Sivashinsky (1970).

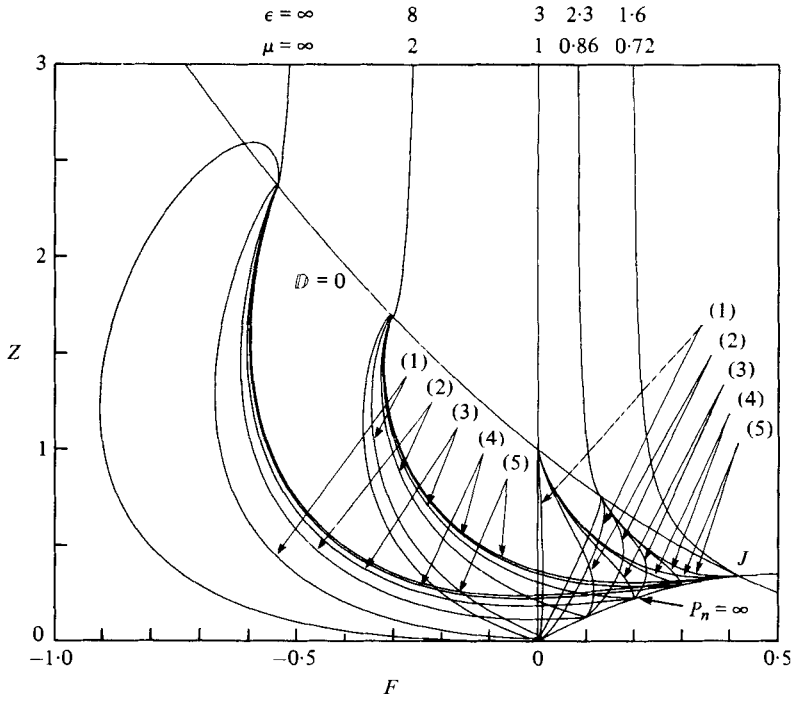

FIGURE 3. Representative integral curves on the phase plane for non-unique solutions ($j = 2$, $\gamma = 1{\cdot}4$).

by the point on the $\mathbb{D} = 0$ line, it becomes sonic. Beyond this point, the integral curve for all the family is the axis between singularities A and D corresponding to states at which the flow is locally subsonic.

For $\epsilon < 3$ (or $\mu < 1$), the front is decelerating, at $\epsilon = 3$ (or $\mu = 1$), it propagates at constant speed while, for $\epsilon > 3$ (or $\mu > 1$), it is accelerating. For the latter, the solutions display another interesting feature due to the fact that, in this domain, the locus of the points of maximum Z, the $\mathbb{P} = 0$ line, having intersected the $\mathbb{D} = 0$ line at the point $F = 0$, $Z = 1$, lies above it. The consequences of this fact are depicted in figure 4 showing, in a much enlarged scale, the integral curve corresponding to the case of $\epsilon = \mu = \infty$ and $F_n = 0{\cdot}1$ ($\omega = 0{\cdot}0247$). The curve has two points on the $\mathbb{D} = 0$ line, neither of which has a physical meaning. The physically meaningful parts are shown by continuous lines. They terminate at two conjugate points satisfying the Rankine–Hugoniot condition, excluding the parts represented by broken lines. *Thus all the blast waves associated with accelerating fronts have an internal discontinuity.*

In general this discontinuity corresponds to an extremely weak shock, the Mach number in the relatively extreme, in this respect, case of figure 4 being just

$$1 + 3{\cdot}8 \times 10^{-5}.$$

Nonetheless, as a consequence of the relative position of the $\mathbb{P} = 0$ and $\mathbb{D} = 0$ lines pointed out above, it must exist in all blast waves with accelerating fronts.

In order to describe the evolution of the flow field for the various cases in more detail, provided here in figures 5–9 are representative space profiles of gasdynamic

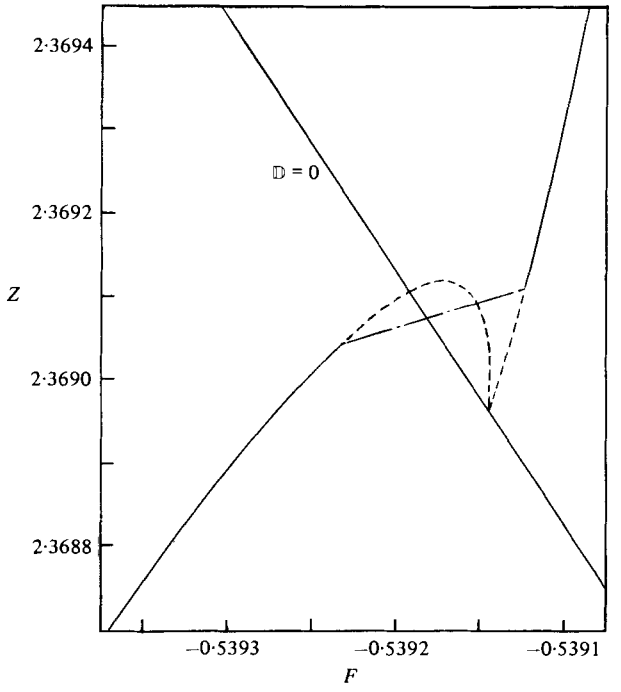

FIGURE 4. Close-up of the discontinuous change of state around the sonic locus of $\mathbb{D} = 0$ in the case of $\epsilon = \mu = \infty$ and $F_n = 0{\cdot}1$ or $\omega = 0{\cdot}22$ ($j = 2$, $\gamma = 1{\cdot}4$).

parameters, namely the particle velocity, u/u_n, temperature, T/T_n, density, ρ/ρ_n, and pressure, p/p_n. Figure 5 displays these profiles for all the unique solutions represented in figure 2. They start with those associated with the Chapman–Jouguet condition established immediately behind the front and terminate with that corresponding to infinite density ratio across it. In the latter case all the mass is actually concentrated at the front since, as it becomes apparent from figure 5(*c*), the density, after attaining infinity behind the front, goes down to zero immediately thereafter.

Space profiles depicted in figures 6–9 correspond to each of the families displayed in figure 3, that is, respectively, to $\epsilon = 2{\cdot}3$, 3, 8, and ∞ (or $\mu = 0{\cdot}86$, 1, 2, and ∞). The various members of each family correspond, as in figure 3, to different values of F_n or ω, from those associated with the Chapman–Jouguet condition immediately behind the front to the limiting case of $F_n = \omega = 0$. Here the whole flow field collapses to a point. Thus, although, as noted before, the front propagates then at infinite velocity, it carries no change of state. The energy is evidently dissipated then in the form of a pure radiation wave without involving any mass motion.

The characteristic features exhibited by space profiles as this limit is approached are as follows:

For $\epsilon_J < \epsilon < j+1$ (or $\mu_J < \mu < 1$), as represented by figure 6, particle velocities tend to infinity behind the front before falling down to zero at the centre, temperatures attain there infinity, densities get down to zero, while the pressure level increases towards infinity.

For $\epsilon = j+1$ (or $\mu = 1$), as shown in figure 7, there is always a core of zero velocity

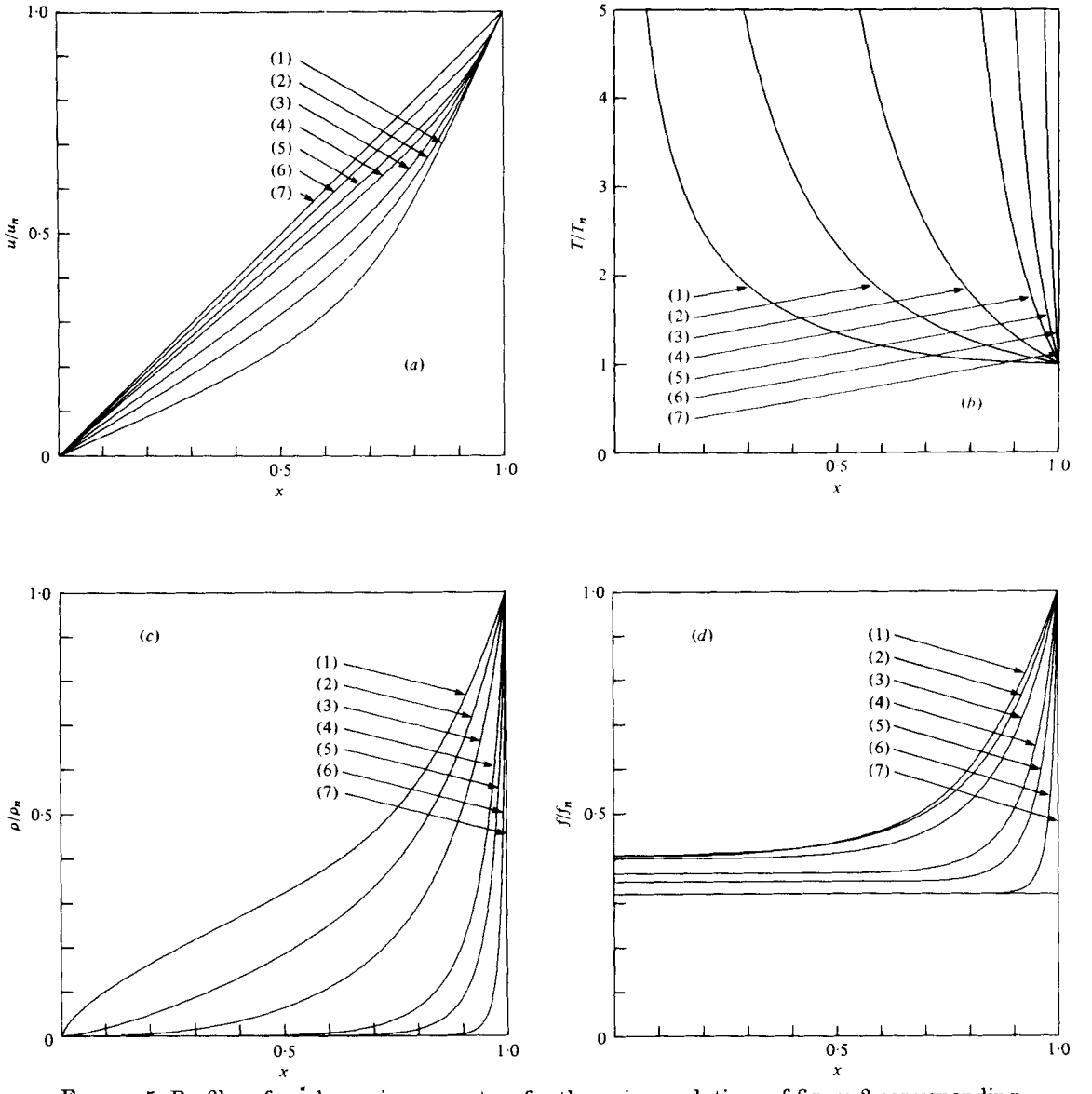

FIGURE 5. Profiles of gasdynamic parameters for the unique solutions of figure 2 corresponding to $-3{\cdot}871 \leqslant \epsilon \leqslant 1{\cdot}6$ or $0{\cdot}3226 \leqslant \mu \leqslant 0{\cdot}72$. (*a*) Particle velocity; (*b*) temperature; (*c*) density; (*d*) pressure. Values of (ϵ, μ) are: (1), (1·6, 0·72); (2), (1·0, 0·6); (3), (0·5, 0·5); (4), (0, 0·4); (5), (−0·15, 0·37); (6), (−0·3, 0·34); (7), (−0·3871, 0·3226).

around the centre, where all the other parameters have to be maintained, of course, at a uniform level. The front of this core is attained when the relative particle velocity with respect to the locus of x = const. becomes equal to the local velocity of sound. As ω falls down to zero the uniform level of all the parameters of state around the centre increases towards unity, so that the state of the medium approaches an

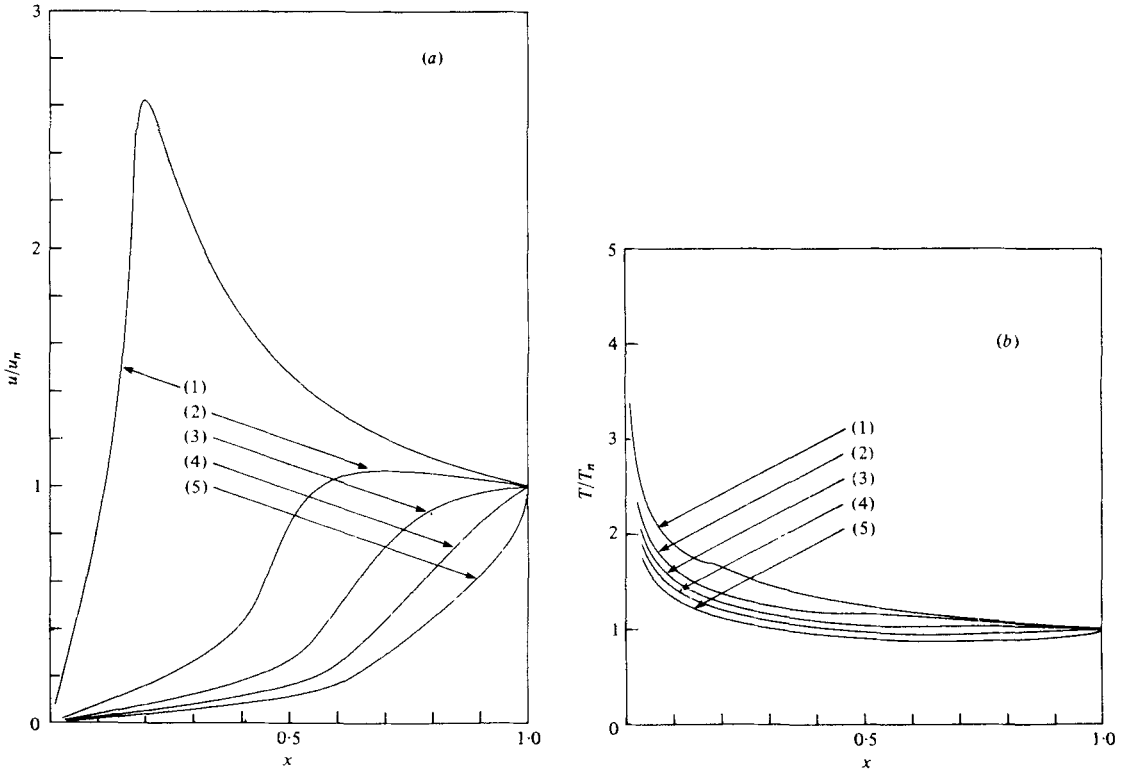

FIGURE 6 (*a*, *b*). For legend see facing page.

undisturbed condition throughout the flow field, causing, in particular, the temperature, density and pressure profiles to look more and more alike.

As illustrated by figures 8 and 9, space profiles of gasdynamic parameters for $\epsilon > j+1$ (or $\mu > 1$), exhibit a radically different behaviour than those for $\epsilon < j+1$ (or $\mu < 1$). Here particle velocities are negative in the core around the centre, temperatures tend to zero, densities approach infinity, while the pressure level at the centre falls down to zero as ω gets closer to its limiting value of $\omega = 0$. As pointed out before, the flow fields of figures 8 and 9 contain an internal discontinuity. Its position is indicated on each profile by a short vertical line. The significance of figure 9 lies in the fact that it represents the limiting condition of $\epsilon = \mu = \infty$. It is of interest to observe here how the velocity tends to the plateau of $u = 0$ throughout the flow field as ω gets down to zero. This is associated with density ratio approaching the level of unity, causing the pressure profile to become more and more similar to that of temperature.

Figure 10 presents the salient parameters of the problem expressed as a function of F_D used as the abscissa in order to accommodate most conveniently the full scope of solutions. The parameters are: the reduced co-ordinate of the front, F_n, determined by the intersection of the integral curve with the line of $P_n = \infty$, and the non-dimensional energy integral, J, evaluated by the use of (35). As indicated at the top, vertical lines correspond to the same values of ϵ and μ as those of figures 2, 3 and 5–9.

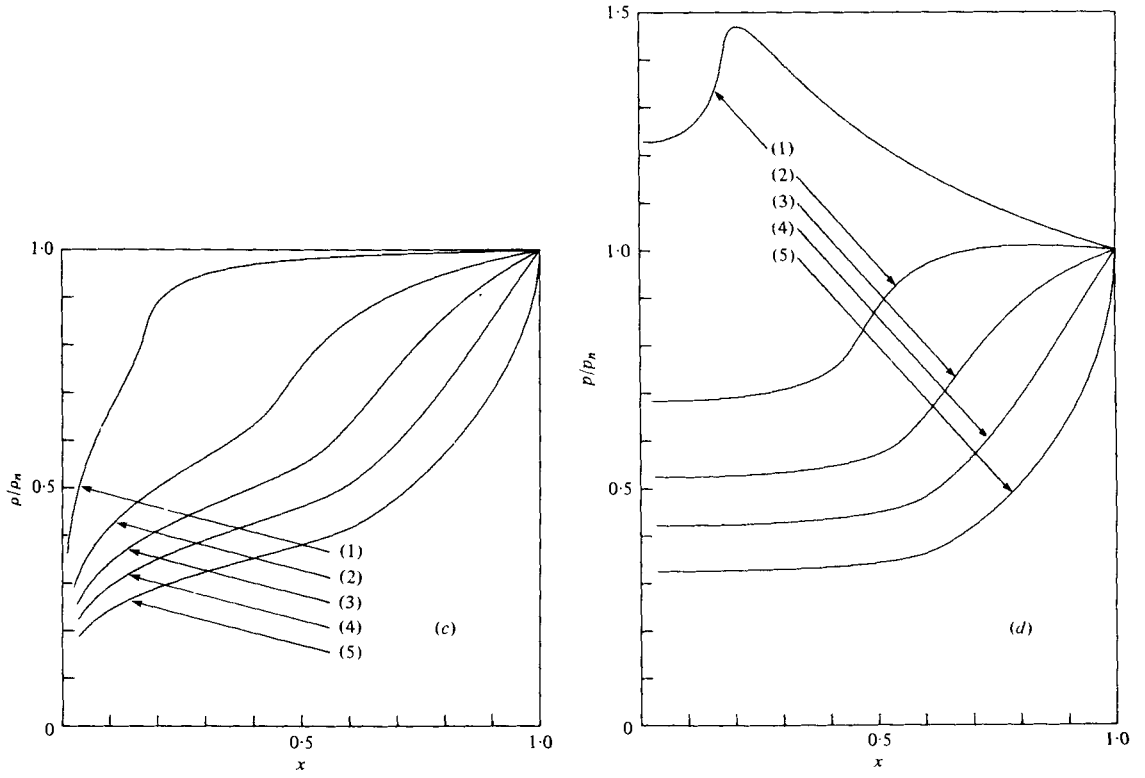

FIGURE 6. Profiles of gasdynamic parameters for the non-unique solutions of figure 3 corresponding to $\epsilon = 2{\cdot}3$ or $\mu = 0{\cdot}86$. (*a*) Particle velocity; (*b*) temperature; (*c*) density; (*d*) pressure. Values of (F_n, ω) are: (1), (0·01, 0·0247); (2), (0·1, 0·22); (3), (0·2, 0·38); (4), (0·3, 0·48); (5), (0·4167, 0·5208).

The parameter F_n is, of course, constant for all the members of different families of non-unique solutions whose integral curves terminate at the same point on the line of $P_n = \infty$. They are represented on figure 10 by horizontal lines. The corresponding energy integrals are displayed by curves, as indicated by zig-zag lines with arrows. They all tend to infinity as ϵ and μ approach their limiting level of $\epsilon = \mu = \infty$.

With the values of F_n and ϵ depicted in figure 10, one can calculate J by the use of (32). The results of this computation were in such good agreement with those shown in figure 10 that the difference between them could not have been demonstrated there pictorially. This completes the check of the accuracy of our results.

4. Conclusions

A parametric study of self-similar solutions for point explosions of variable energy has been presented. The scope of the coverage is bound by two conditions of infinity, on one side that in the rate of energy deposition and, on the other, by that in the density ratio across the front. Within this regime, blast waves associated with both energy gain and loss are included, the solution for adiabatic strong explosion providing the line of demarcation between the two.

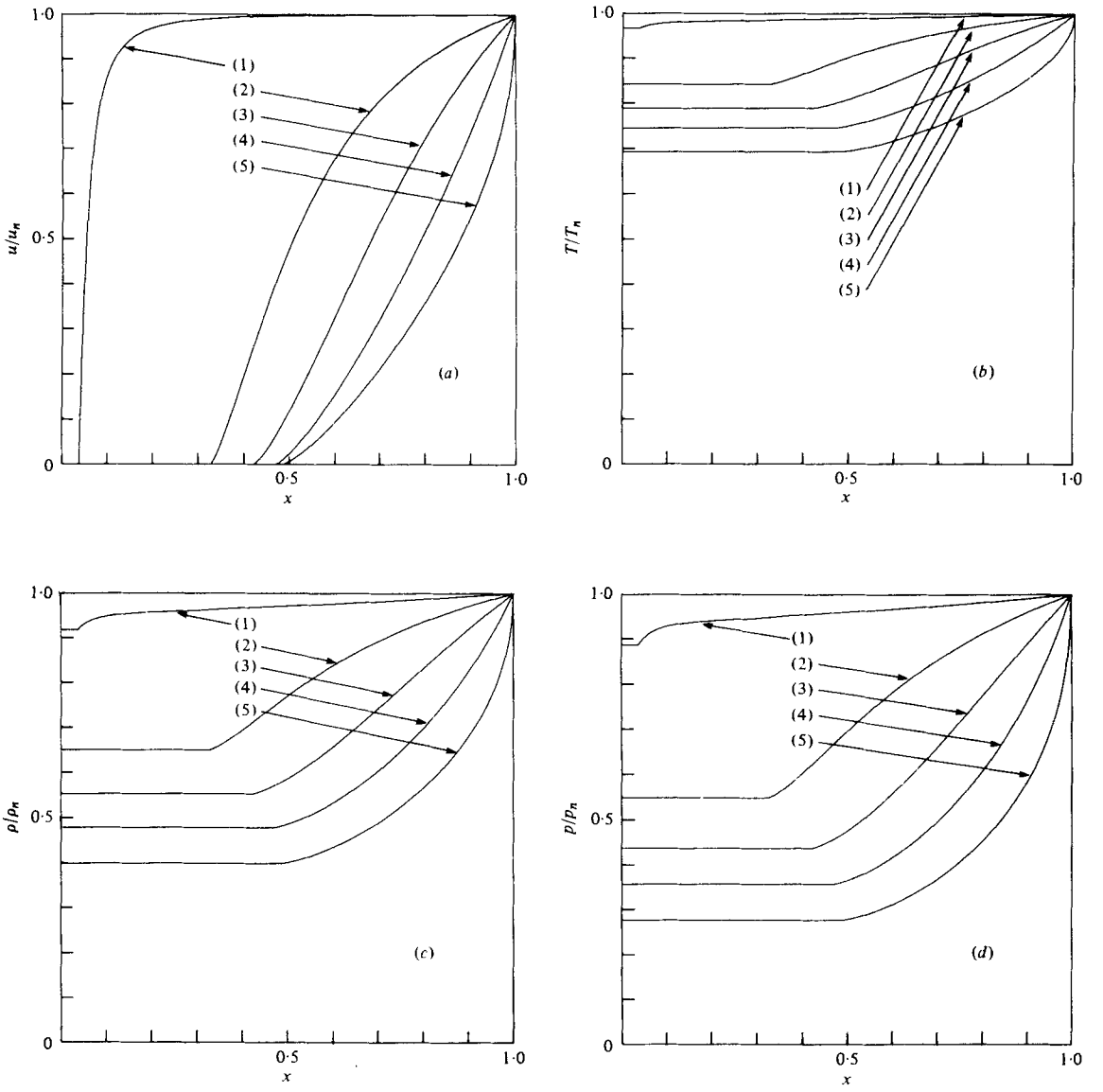

FIGURE 7. Profiles of gasdynamic parameters for the non-unique solutions of figure 3 corresponding to $\epsilon = 3$ or $\mu = 1$. (*a*) Particle velocity; (*b*) temperature; (*c*) density; (*d*) pressure. Values of (F_n, ω) are as in figure 6.

The primary parameter of the study is the wave-power index, ϵ, indicating the rate of energy deposition – a quantity related linearly to the front-velocity index, μ, describing the curvature of the front trajectory in the time–space domain. Starting with the value of ϵ corresponding to the lowest rate of energy gain compatible with the Chapman–Jouguet condition established immediately behind the front, solutions are no more uniquely dependent on this parameter. For the same value of ϵ (and μ) one can have a set of solutions corresponding to either sonic or supersonic flow immediately

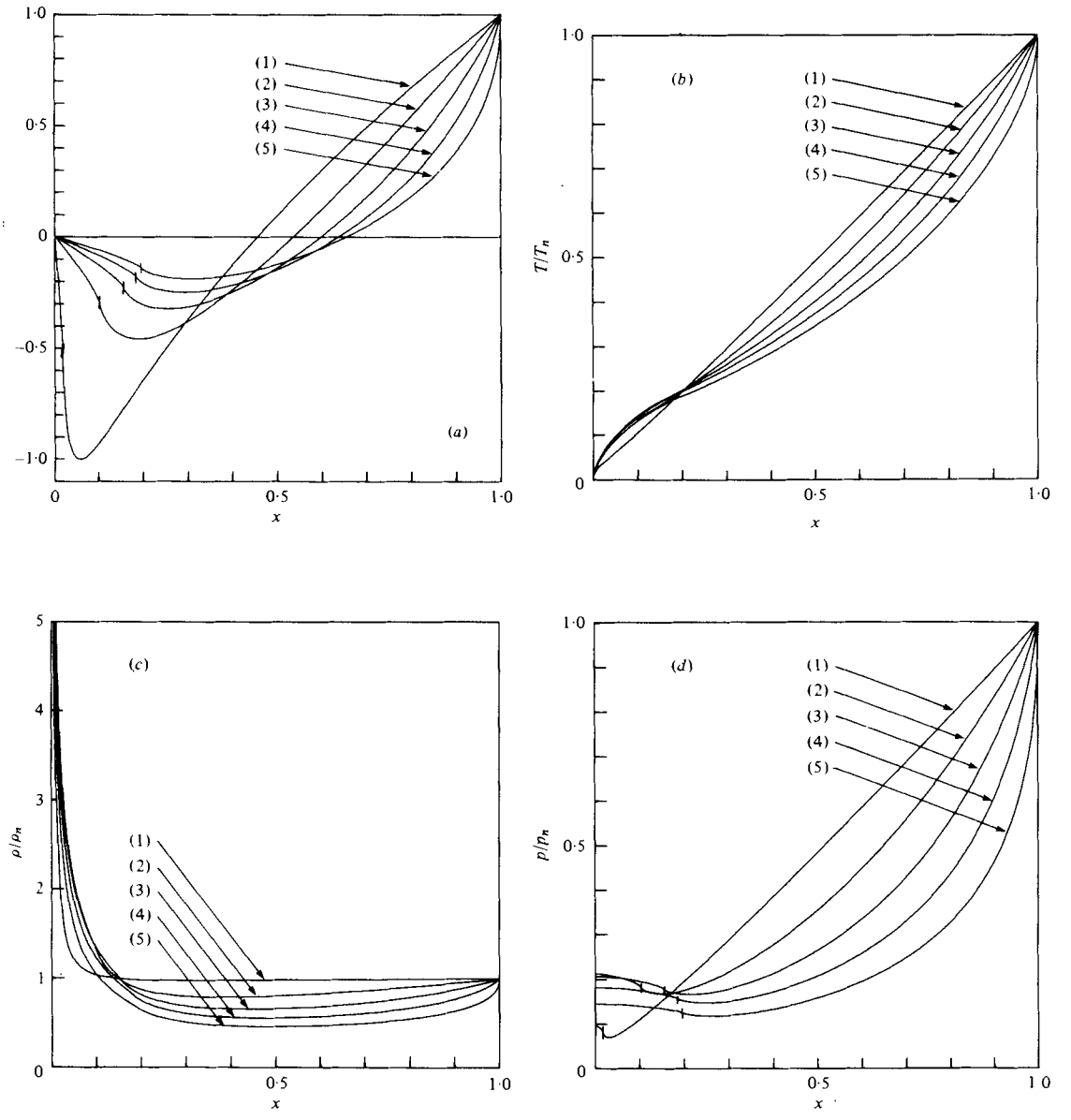

FIGURE 8. Profiles of gasdynamic parameters for the non-unique solutions of figure 3 corresponding to $\epsilon = 8$ or $\mu = 2$. (*a*) Particle velocity; (*b*) temperature: (*c*) density; (*d*) pressure. Values of (F_n, ω) are as in figure 6.

behind the front. This is followed by a regime of locally supersonic flow. While the transition to subsonic flow is smooth for $\epsilon < j+1$ (or $\mu < 1$), that is in blast waves with decelerating fronts, it is in principle discontinuous for $\epsilon > j+1$ ($\mu > 1$), that is in blast waves with accelerating fronts. For $\epsilon = j+1$ (or $\mu = 1$), that is in blast waves with constant velocity fronts, the flow is locally supersonic except for a central core of uniform state at rest which is established when the flow becomes locally sonic.

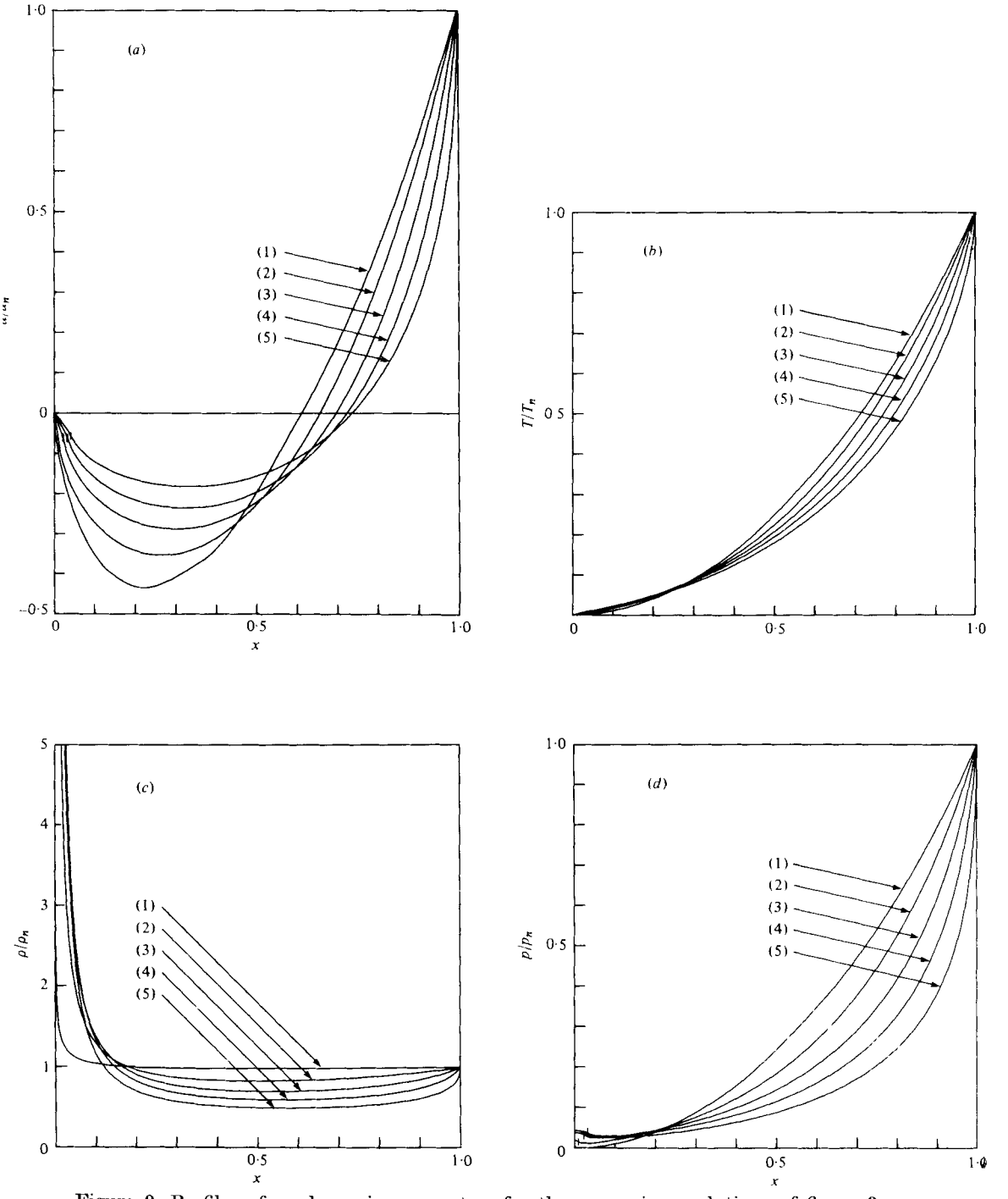

Figure 9. Profiles of gasdynamic parameters for the non-unique solutions of figure 3 corresponding to $\epsilon = \mu = \infty$. (*a*) Particle velocity; (*b*) temperature; (*c*) density; (*d*) pressure. Values of (F_n, ω) are as in figure 6.

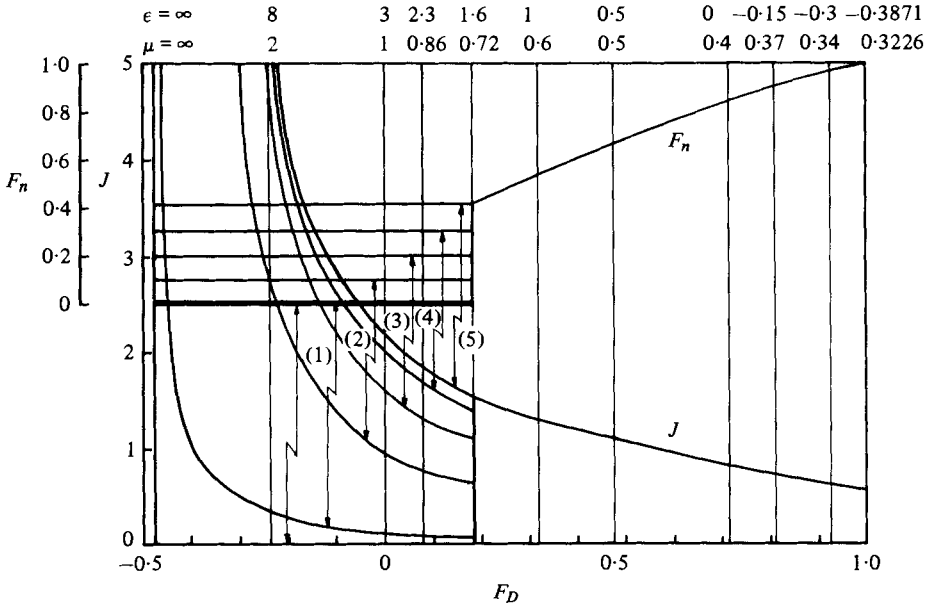

FIGURE 10. Salient parameters of the problem, the reduced co-ordinate of the front, F_n, and the non-dimensional energy integral, J, in relation to the wave power index, ϵ, and the front velocity index, μ.

This work was supported in part by the U. S. Army Research Office under ARO Grant DAAG 29-77-G-0064; by the National Science Foundation under NSF Grant ENG 78-12372; and by the U.S. Department of Energy under Contract W-7405-ENG-48.

REFERENCES

BARENBLATT, G. I. & SIVASHINSKY, G. I. 1970 Self-similar solutions of the second order in the problem of the propagation of strong blast waves. *Prikl. Matem. i Mekh.* **34**, 685–692.

BARENBLATT, G. I. & ZEL'DOVICH, YA. B. 1971 Intermediate asymptotics in mathematical physics. *Prog. Math. Sci.* **26**, 115–129 (in Russian).

BARENBLATT, G. I. & ZEL'DOVICH, YA. B. 1972 Self-similar solutions as intermediate asymptotics. *Ann. Rev. Fluid Mech.* **4**, 285–312.

CHAMPETIER, J. L., COUAIRON, M. & VENDENBOOMGAERDE, Y. 1968 Sur les boules de claquage créées par lasers. *C. R. Acad. Sci. Paris* **267**, 1133–1136.

COURANT, R. & FRIEDRICHS, K. O. 1948 *Supersonic Flow and Shock Waves*. Wiley.

DABORA, E. K. 1972 Variable energy blast waves. *A.I.A.A. J.* **10**, 1384–1386.

FREEMAN, R. A. 1968 Variable energy blast waves. *J. Phys.* D, *Appl. Phys.* **1**, 1697–1710.

GUDERLEY, G. 1942 Powerful spherical and cylindrical compression shocks in the neighborhood of the center of the sphere and of the cylinder axis. *Luftfahrtforschung* **19**, 302–312.

NEUMANN, J. VON 1963 The point source solution, *N.D.R.C., Div.* B *Rep.* AM-9 (classified report written in 1941 and published in *John von Neumann Collected Works*, vol. VI (ed. A. H. Taub), pp. 219–237. Pergamon).

OPPENHEIM, A. K., KUHL, A. L. & KAMEL, M. M. 1972 On self-similar blast waves headed by the Chapman–Jouguet detonation. *J. Fluid Mech.* **55**, 257–270.

OPPENHEIM, A. K., KUHL, A. L., LUNDSTROM, E. A. & KAMEL, M. M. 1972 A parametric study of self-similar blast waves. *J. Fluid Mech.* **52**, 657–682.

RAIZER, YU. P. 1974 The laser spark. *Izd. Nauka*, Moscow (in Russian).

SEDOV, L. I. 1945 On some non-steady-state motions of a compressible fluid. *Prikl. Mat. i Mech.* **9**, 285–311.

SEDOV, L. I. 1946 Propagation of intense blast waves. *Prikl. Mat. i. Mech.* **10**, 2.

SEDOV, L. I. 1957 *Similarity and Dimensional Methods in Mechanics*, 4th edn, Moscow (Translated 1959 (ed. M. Holt). Academic).

TAYLOR, G. I. 1950*a* The formation of a blast wave by a very intense explosion. *British Rep.* RC-210 (classified report written in 1941 and published in *Proc. Roy. Soc.* A **201**, 175–186).

TAYLOR, G. I. 1950*b* The dynamics of the combustion products behind plane and spherical fronts in explosives. *Proc. Roy. Soc.* A **200**, 235–247 (see also 1958 *Fundamentals of Gasdynamics* (ed. H. W. Emmons), cha. 3. Princeton University Press).

WILSON, C. R. & TURCOTTE, D. L. 1970 Similarity solution for a spherical radiation-driven shock wave. *J. Fluid Mech.* **43**, 399–406.

ZEL'DOVICH, YA. B. 1942 On the distribution of pressure and velocity in the product of a detonation blast, particularly with the propagation of a spherical detonation wave. *Zh. Exp. i Teor. Fiz.* **12**, 9.

ZEL'DOVICH, YA. B. & KOMPANEETS, A. S. 1955 *Teoriya Detonatsii.* Moscow: Gostekhizdat (Translation 1960 *Theory of Detonation.* Academic).

ZEL'DOVICH, YA. B. & RAIZER, YU. P. 1966 *Physics of Shock Waves and High Temperature Hydrodynamic Phenomena*, 2nd edn, p. 686. Moscow: Izdatel'stuo Nauka (Translation 1967 (ed. W. D. Hayes & R. F. Probstein). Academic).